Deep Capillary Plexus Features in Acute Macular Neuroretinopathy: Novel Insights Based on the Anatomy of Henle Fiber Layer

Diogo Cabral,[1,2] Prithvi Ramtohul,[1] Luca Zatreanu,[3] Daniel Galhoz,[2,4] Miguel Leitao,[5] Vanda Nogueira,[5] David Sarraf,[6] and K. Bailey Freund[1,7]

[1]Vitreous Retina Macula Consultants of New York, New York, New York, United States
[2]iNOVA4Health, NOVA Medical School, Universidade NOVA de Lisboa, Lisbon, Portugal
[3]Rochester Regional Health, Rochester, New York, United States
[4]Instituto Superior Tecnico, Universidade de Lisboa, Lisbon, Portugal
[5]Instituto de Oftalmologia Dr. Gama Pinto, Lisbon, Portugal
[6]Retinal Disorders and Ophthalmic Genetics Division, Stein Eye Institute, University of California, Los Angeles, Los Angeles, California, United States
[7]Department of Ophthalmology, NYU Grossman School of Medicine, New York, New York, United States

Correspondence: K. Bailey Freund, Vitreous Retina Macula Consultants of New York, 950 Third Ave. New York, NY 10022, USA; kbfreund@gmail.com.

Received: August 10, 2022
Accepted: November 13, 2022
Published: December 5, 2022

Citation: Cabral D, Ramtohul P, Zatreanu L, et al. Deep capillary plexus features in acute macular neuroretinopathy: Novel insights based on the anatomy of Henle fiber layer. *Invest Ophthalmol Vis Sci.* 2022;63(13):4. https://doi.org/10.1167/iovs.63.13.4

Purpose. The purpose of this study was to identify a precise location of deep capillary plexus (DCP) injury in acute macular neuroretinopathy (AMN) lesions using multimodal imaging.

Methods. En face structural optical coherence tomography (OCT) images were manually segmented to delineate outer retinal AMN lesions involving the ellipsoid zone and interdigitation zone. AMN lesion centroid was calculated, and image distortion was applied to correct for Henle fiber layer (HFL) length and orientation. The resulting image was registered with the corresponding en face OCT angiography (OCTA) image segmented at the DCP and structural OCT volume before grading for vascular and structural features, respectively.

Results. Thirty-nine AMN lesions from 16 eyes (11 female patients, mean age 34 ± 4 years) were analyzed. After correcting for HFL anatomy, in 62% of AMN lesions, the centroid co-localized with a capillary vortex (pattern 1); flow defects were detected in 33% of lesions (pattern 2); and in 5% of lesions no specific pattern could be identified (pattern 3). The detection of a specific pattern increased after correcting the projection of AMN lesion for HFL anatomy (28% vs. 5%, $P = 0.04$). Outer nuclear layer thickness was lower in the centroid area in 10 (29%) AMN lesions from 6 patients, all corresponding to lesions fitting pattern 2 ($r = 0.78$, $P < 0.001$).

Conclusions. AMN lesions might be a result of DCP impairment at the level of the capillary vortex or draining venule. In eyes with AMN, the location of outer retinal changes associated with DCP ischemia appears to be influenced by the length and orientation of HFL.

Keywords: acute macular neuroretinopathy (AMN), Henle's fiber layer (HFL), deep capillary plexus (DCP), optical coherence tomography angiography (OCTA)

Acute macular neuroretinopathy (AMN) is a rare condition, first reported by Bos and Deutman[1] who described a case series of young women with paracentral scotomas corresponding to dark-reddish, wedge-shaped macular lesions in ophthalmoscopy. Multimodal imaging enabled increased detection sensitivity of this entity and provided important insights into the associated structural retinal changes. Corver et al.[2] showed an enhanced detection of AMN lesions using confocal scanning laser ophthalmoscopy infrared reflectance (SLO-IR; 810 nm). Using time-domain optical coherence tomography (OCT), Feigl and Hass[3] showed that, contrary to initial belief, AMN lesions seemed to be confined to the outer retinal layers rather than the superficial layers.[4] Analyzing the OCT features of 2 patients examined within the first 2 days of symptom-onset, Fawzi et al. observed that outer plexiform layer (OPL) hyperreflectivity preceded the disruption of outer photoreceptor bands and subsequent outer nuclear layer (ONL) thinning.[5] In a case report of a 26-year-old woman with paracentral scotomas secondary to AMN, Hansen et al. demonstrated an excellent anatomic correspondence among areas of reduced microperimetry sensitivity, SLO-IR hyporeflectivity, attenuation of spectral domain OCT (SD-OCT) band #2 (the ellipsoid zone [EZ] or inner segment/outer segment [IS/OS] junction), and OCT band #3 (the "OS/RPE" - now called the interdigitation zone [IZ]), and selective cone photoreceptor

(as opposed to rod) loss with adaptive optics scanning light ophthalmoscopy.[6]

The retinal OPL is composed of synapses among photoreceptors, bipolar cells, and horizontal cells.[7] This region has a high concentration of photoreceptor mitochondria and is sustained by the deep capillary plexus (DCP).[8,9] The photoreceptors' axons, together with outer Müller cell processes, form the Henle fiber layer (HFL). The HFL is obliquely oriented in relation to the photoreceptor outer segments (OS) within the central 15 degrees of the macula because of both foveal pit development and IS/OS squeezed together while the large cone pedicles are attached to the centrifugally spreading bipolar cells.[10,11] Therefore, in the perifovea, bipolar and ganglion cells are displaced from the position of the photoreceptors that feed the receptive field center.[12] Damage to the OPL can result in photoreceptor axon injury, which in turn can produce OS disruption that is laterally displaced from the site of OPL injury. The advent of OCT angiography (OCTA) has increased our understanding of AMN, with some studies suggesting a role of DCP ischemia in AMN.[5,13] However, to the best of our knowledge, the impact of the radially oriented HFL on the areas of OS disruption has not been described.[5,11] In this study, we aimed to explore the effect of HFL length and orientation on the location of outer retinal changes resulting from DCP ischemia in eyes with AMN.

Methods

This was a retrospective case series from three tertiary retina referral centers. Written informed consent was obtained from each participant and local institutional review board approval was obtained from the Western Institutional Review Board (Olympia, WA, USA) and Comissão de Ética para a Saúde do Instituto de Oftalmologia Dr. Gama Pinto (Lisbon, Portugal). A waiver was also granted from the University of Rochester Ethics Committee (Rochester, NY, USA) for the retrospective usage of anonymized data acquired during routine clinical practice. This study adhered to the tenets of the Declaration of Helsinki and complied with the Health Insurance Portability and Accountability Act of 1996.

Inclusion criteria consisted of patients with a clinical diagnosis of AMN imaged with dense structural OCT volumes (interscan distance 11–30 µm) and OCTA (interscan distance 6 or 10 µm) covering the full extent of each AMN lesion. The diagnostic criteria for AMN included a history of one or more acute paracentral scotoma corresponding to hyporeflectivity with near infrared reflectance (NIR) and hyperreflectivity of the ONL associated with EZ and IZ disruption with OCT. Exclusion criteria consisted of eyes with retinal diseases other than AMN and specific AMN lesions with a diameter larger than one average disk diameter.[14] A cutoff value for specific AMN lesions size was used given that larger lesions may represent the confluence of multiple smaller ones, which could confound a precise analysis of DCP features per AMN lesion.[5]

For each eligible patient, the complete medical records were reviewed. Data collection included patient age, sex, concomitant systemic and ocular disorders, medications, and baseline Snellen visual acuity (VA) using the Snellen chart. Snellen VA was converted to logarithm of the minimum angle of resolution (logMAR) for statistical analysis. All patients underwent complete ophthalmologic examinations, including slit lamp biomicroscopy, ophthalmoscopy, and multimodal retinal imaging. NIR and SD-OCT were acquired using the SPECTRALIS OCT (Heidelberg Engineering, Heidelberg, Germany). Four patients (36%) also underwent high resolution (High-Res OCT; Heidelberg Engineering) with 3 µm axial resolution. OCTA was acquired using the High-Res OCT device, the PLEX Elite 9000 (Carl Zeiss Meditec, Inc., Dublin, CA, USA) and/or the Avanti RTVue XR (Optovue Inc., Fremont, CA, USA). AMN lesions were identified based on structural OCT B-scans from the first evaluation. The OCTA and structural OCT from the last observation were considered for the analysis of DCP features and evaluation of ONL thickness, respectively.

Each OCTA and structural OCT study was reviewed and automated segmentations of the OPL, external limiting membrane (ELM), EZ, and IZ were verified and manually corrected, when needed. OCTA projection artifacts were removed using the manufacturer's algorithms and the en face images of the DCP were exported. With structural OCT B-scans, an ONL thickness map (distance between OPL and ELM) was exported and en face structural OCT was manually segmented to evaluate the reflectivity of the photoreceptor OS (segmentation between EZ and IZ). NIR, en face OCTA, ONL thickness maps, and en face OCT images were registered using the plugin Landmark Correspondences for Fiji (US National Institutes of Health, Bethesda, MD, USA) by selecting six corresponding points for each pair of images and using a similarity algorithm.[15] The resulting aligned en face OCT images were used to manually segment areas of EZ/IZ disruption using the pencil tool of Fiji. The centroid of AMN lesions was identified using the "centroid script" command, and the area of each lesion was transformed with respect to HFL anatomy, using a code designed in MATLAB version R2019b (The MathWorks Inc., Natick, MA, USA 2019). The code used to transform the images is publicly available.[16] HFL length and orientation were calculated along the horizontal meridian for each point of the segmented region, as previously described by Drasdo et al. (Drasdo displacement).[10] Radial displacement values for any other meridians were obtained by a linear interpolation between values of the horizontal meridian with the same distance from the foveal center in a polar coordinate system. Finally, processed images were merged into 3 distinct composites per eye: image composite 1 (NIR + OCTA + AMN lesions); image composite 2 (NIR + OCTA + transformed AMN lesions); and image composite 3 (NIR with ONL thickness maps + AMN lesions). A graphical representation of the different image processing steps is shown in Supplementary Figure S1.

The investigational version v.6.12.4.710 of Heidelberg Eye Explorer (Heidelberg Engineering) was used for registration of structural OCT with image composite and for grading purposes. AMN lesions were categorized according to their shape (wedge versus round-shaped) and size (larger or smaller than half a standardized disk diameter — i.e. medium or small, respectively). OCTA images were evaluated for the presence of capillary vortices or flow defects spanning the centroid of AMN lesions. Structural OCT horizontal and vertical B-scans were inspected for draining venules or absence of capillaries within AMN lesions. Draining venules were defined using structural OCT as large vessels (diameter ≥15 µm) traversing the inner nuclear layer (INL) with a vertical or oblique orientation angled toward a superficial vessel.[17] The INL/OPL boundary was compared among AMN lesions and other areas to inspect for the absence of DCP capillaries (i.e. round-shaped

Investigative Ophthalmology & Visual Science

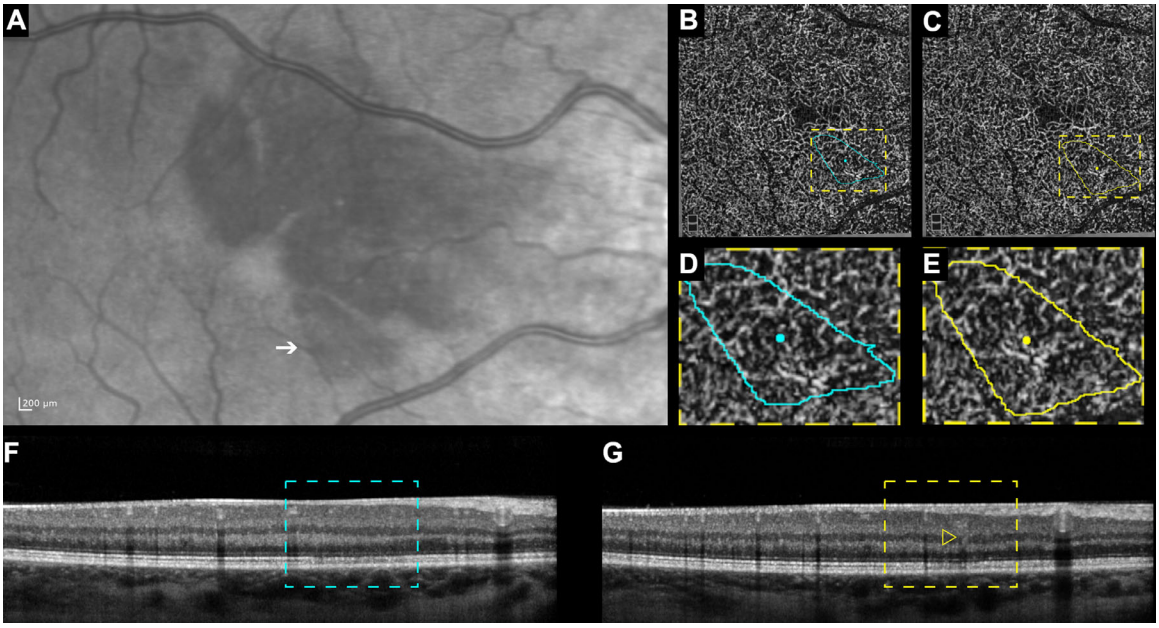

Figure 1. Correcting for Henle's fiber layer (HFL) anatomy when correlating deep capillary plexus (DCP) features with changes in inner segment photoreceptor anatomy. (**A**) In an eye with acute macular neuroretinopathy (AMN), hyporeflective lesions on near-infrared reflectance (NIR) correspond to areas of inner segment photoreceptor disruption. DCP features of a lesion measuring less than one average disk diameter (*white arrow*) were further analyzed with superimposed en face OCTA of the DCP (**B**, **C**) with corresponding magnified insets (**D**, **E**). **D** AMN lesion (cyan contour) direct projection on the DCP, without accounting for HFL anatomy, fails to show a draining venule near the lesion centroid (cyan dot). **E** After correcting the projection of the AMN lesion for HFL anatomy (*yellow contour*), there is a convergence of DCP capillaries near the lesion centroid (*yellow dot*). (**F**) OCT B-scan spanning the centroid of AMN lesion uncorrected for HFL anatomy shows ellipsoid zone (EZ) and interdigitation zone (IZ) disruption in the absence of specific DCP features (*cyan inset*). (**G**) After accounting for HFL anatomy, the OCT B-scan shows a draining venule (*yellow arrow*) crossing the inner nuclear layer in the centroid of the AMN lesion (*yellow inset*).

hyperreflective structures seen with OCT B-scans). Structural OCT and OCTA were evaluated by two groups of graders (image composite 1 = ML and VN and image composites 2 and 3 = DC and PR). Disagreements over readings were resolved by open adjudication. Figure 1 shows an example of the impact of correcting an AMN lesion for HFL length and orientation while grading DCP features. The distribution of ONL thickness in AMN lesions was evaluated in color-coded maps using the plot profile function of Fiji. The intensities of the pixels corresponding to ONL thickness were evaluated in the centroidal axes (major and minor). When the distribution of values followed a U-shape in both axes, the centroid was considered to have a lower ONL thickness than the rest of the lesion. An example of the evaluation process of ONL thickness is available in Supplementary Figure S2.

An exploratory analysis of the demographic, clinical, and imaging features was conducted. Continuous variables are presented as mean ± standard deviation (SD) or median ± interquartile range (25th percentile and 75th percentile), as appropriate. The distribution of categorical variables in distinct samples was compared using the chi squared test. The kappa statistic was used to test inter-rater reliability and Spearman's rank correlation coefficient used to evaluate the strength and direction of association between two ranked variables. Statistical analyses were performed using IBM SPSS Statistics for Windows, version 25.0 (IBM Corp., Armonk, NY, USA).

Results

A total of 39 AMN lesions from 16 eyes (11 female patients) were evaluated. The mean age in the cohort was 34 ± 4 years (range = 20–50 years). The mean BCVA was 0.10 ± 0.06 logMAR (range = 0–1 logMAR; Snellen equivalent 20/25). The median interval between onset of symptoms and first evaluation was 12 days (interquartile range = 6–42 days). In 3 patients, the first evaluation was within the first 5 days after symptoms onset (early AMN). The median follow-up between diagnosis and last examination was 8 weeks (interquartile range = 6–23 weeks). In 6 cases (55%), AMN occurred within 2 weeks after a presumed viral infection, and 7 patients (64%) were taking oral contraceptive medications. The Table summarizes demographic and clinical findings.

For the purpose of statistical analysis, imaging findings were grouped into 3 patterns: pattern 1 = capillary vortex at the centroid of the AMN lesion with OCTA and a corresponding draining venule arising from the center of the vortex with structural OCT B-scan (Fig. 2); pattern 2 = flow defect at the centroid of the AMN lesion with OCTA and undetectable capillaries with structural OCT B-scan (Fig. 3); and pattern 3 = lesions in which no specific pattern could be found.

Analysis of AMN lesions after correction for HFL anatomy (image composite 2) showed that 24 lesions (62%) fit pattern 1 and 13 lesions (33%) fit pattern 2. In two cases (5%), a specific pattern could not be assigned (pattern 3). In cases graded as pattern 2, the projection of corrected AMN lesions was encircled by capillary vortices in all cases (Fig. 4).

The comparison between the grading of image composite 1 (NIR + OCTA + non-transformed AMN lesion) and composite 2 (NIR + OCTA + transformed AMN lesion) showed a strong level of agreement (kappa = 0.831, $P <$

Table. Demographic and Clinical Data

Case no.	Age, y	Sex	Eye of Lesion	AMN Lesions Number*	Baseline Visual Acuity OD	Baseline Visual Acuity OS	Interval Between First Symptoms and Imaging, d	Interval Between First Symptoms and Last Visit, wk	Recent Viral-Like Illness†	Oral Contraceptives	Systemic Diseases
1	23	F	OU	3	20/20	20/20	5	5	Yes	Yes	None
2	30	F	OU	1	20/20	–	3	8	Yes	Yes	None
3	41	F	OU	4	20/60	20/200	12	271	Yes	Yes	None
4	20	F	OU	3	20/20	20/25	42	6	No‡	Yes	None
5	33	F	OS	3	–	20/20	7	23	No	Yes	None
6	38	F	OS	3	–	20/25	17	48	No	Yes	Sarcoidosis
7	50	F	OD	1	20/20	–	7	19	No	Yes	None
8	34	F	OU	4	20/20	20/20	51	7	Yes	No	None
9	27	F	OU	9	20/20	20/20	5	13	Yes	Yes	None
10	33	F	OS	3	–	20/20	56	8	Yes	Yes	Sjögren Syndrome
11	44	F	OD	1	20/30	–	6	15	No	No	None

AMN, acute macular neuroretinopathy; F, female; OU, oculus uterque; OS, oculus sinister; OD, oculus dexter.
* AMN lesions with a size inferior to one standard disk diameter (1500 µm).
† Patient reported presumed acute viral-like illness (unexplained fever and/or dehydration managed conservatively or with non-steroidal anti-inflammatory drugs) in the 2 weeks preceding AMN symptoms.
‡ Positive polymerase chain reaction test for coronavirus disease 2019 (COVID-19) 2 weeks prior to AMN first symptoms.

0.01) for both pattern 1 and pattern 2 lesions. There was a significant decrease in the prevalence of pattern 3 lesions after correcting for HFL anatomy (12 [28%] vs. 2 [5%], $P = 0.04$).

The ONL thickness map was evaluated in 35 out of the 39 AMN lesions from 9 patients with a follow-up period longer than 6 weeks. For 10 of these lesions (29%) from 6 patients, ONL thickness was lower in the centroid area compared to any other part of the AMN lesion (Fig. 5). All of these lesions corresponded to pattern 2 ($r = 0.78$, $P < 0.001$). In the remaining 25 lesions, we did not find a specific pattern of ONL thickness distribution.

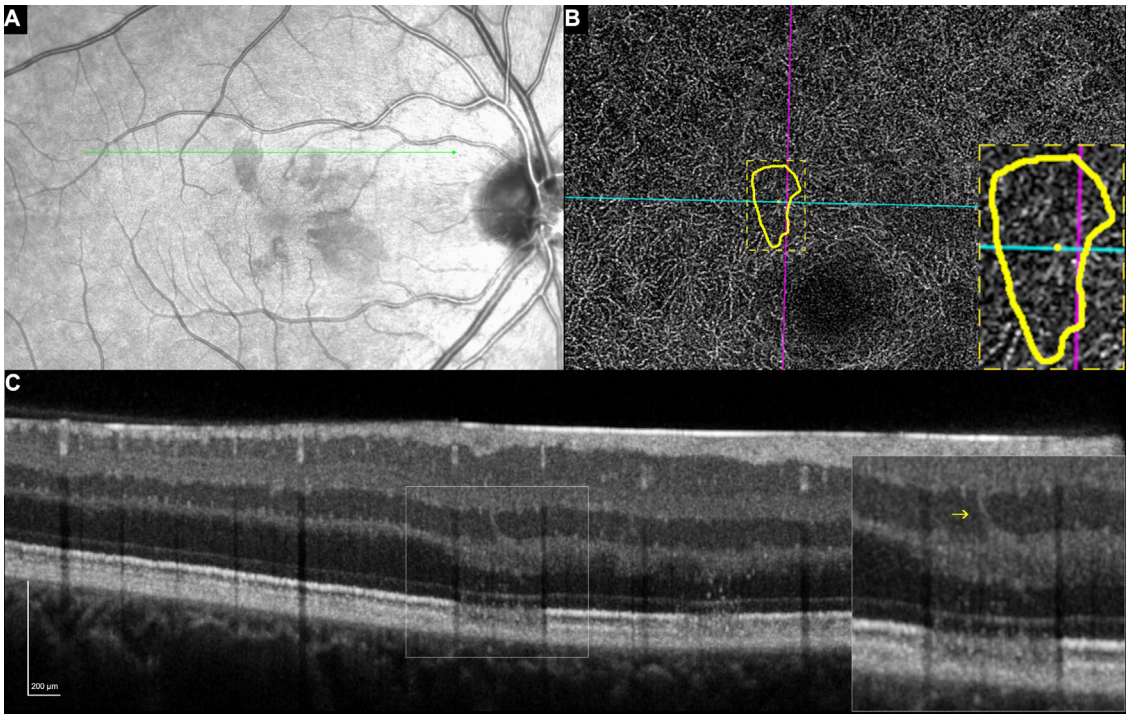

Figure 2. Acute macular neuroretinopathy (AMN) pattern 1: convergence of deep capillary plexus (DCP) capillaries at the lesion centroid. (**A**) Near infrared reflectance image shows multiple AMN lesions. The green arrow indicates the area corresponding to the high-resolution OCT B-scan. (**B**) The image of the DCP shows the projection of one of the AMN lesions corrected for Henle's fiber layer anatomy (*yellow*). A magnified view of the OCTA image (*inset*) shows a convergence of capillaries at the centroid of the AMN lesion (*yellow dot*). (**C**) A high-resolution OCT B-scan spanning the centroid of the AMN lesion shows a draining venule arising from the AMN lesion (*inset*). The DCP draining venule is identified by the *yellow arrow* (*i*nset). The presence of the central draining venule may indicate reperfusion after initial DCP impairment.

Investigative Ophthalmology & Visual Science

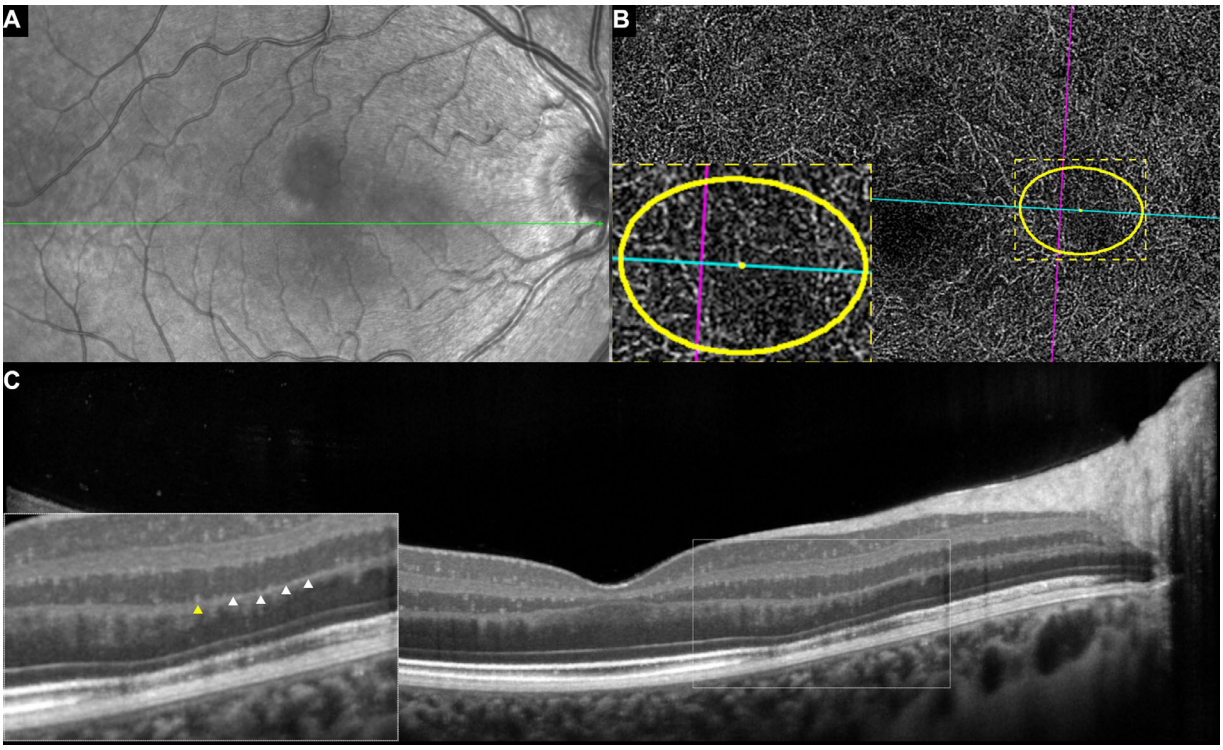

Figure 3. Acute macular neuroretinopathy (AMN) pattern 2: absence of deep capillary plexus (DCP) capillaries at the lesion centroid. (**A**) Near infrared reflectance image of the fundus shows two hyporeflective round-shaped AMN lesions. The *green arrow* indicates the area corresponding to the high-resolution OCT B-scan. (**B**) The image of the DCP shows the projection of the AMN lesions corrected for Henle's fiber layer anatomy (*yellow*). A magnified view of the inset from the OCTA shows a flow defect near the centroid (*yellow dot*) of the AMN lesion. (**C**) High-resolution OCT B-scan through the centroid of the AMN lesion shows the conspicuous absence of capillaries at the level of the posterior inner nuclear layer (corresponding to the DCP) overlying the AMN lesion (*inset*; capillary bare area, *white arrowheads*). For comparison, normal DCP capillaries (*yellow arrowheads*, *inset*) can be seen directly to the left and right of the capillary bare area of the AMN lesion (*white arrowheads*, *inset*). The absence of the central draining venule indicates a more severe DCP perfusion deficit.

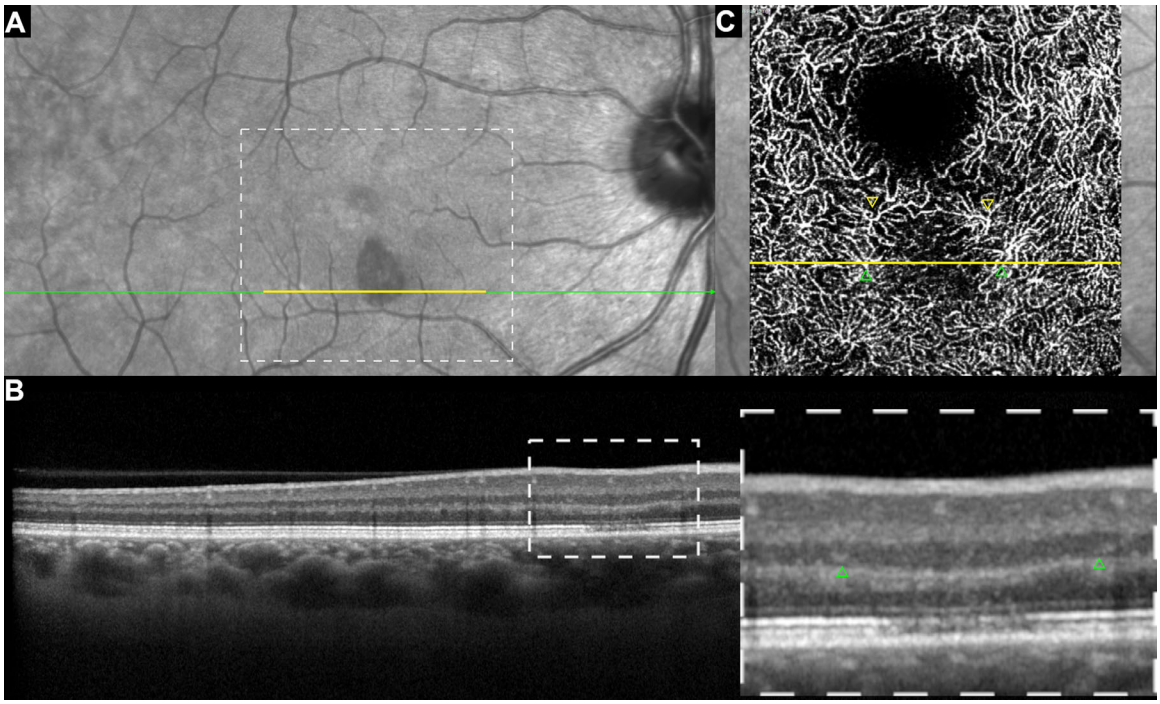

Figure 4. Acute macular neuroretinopathy (AMN) pattern 2: demonstrating encircling of the lesion by capillary vortices of the deep capillary plexus (DCP). (**A**) A near infrared reflectance image of the fundus shows one petaloid-shaped hyporeflective AMN lesion. The *green arrow* indicates the area corresponding to the OCT B-scan. (**B**) An OCT B-scan spanning the centroid of the AMN lesion shows a capillary bare area surrounded by two draining venules (*green arrowheads*, *inset*). (**C**) En face optical coherence tomography-angiography (OCTA) image of the DCP shows various capillary vortices (*colored arrowheads*) encircling the flow defect at the centroid of the AMN lesion.

Investigative Ophthalmology & Visual Science

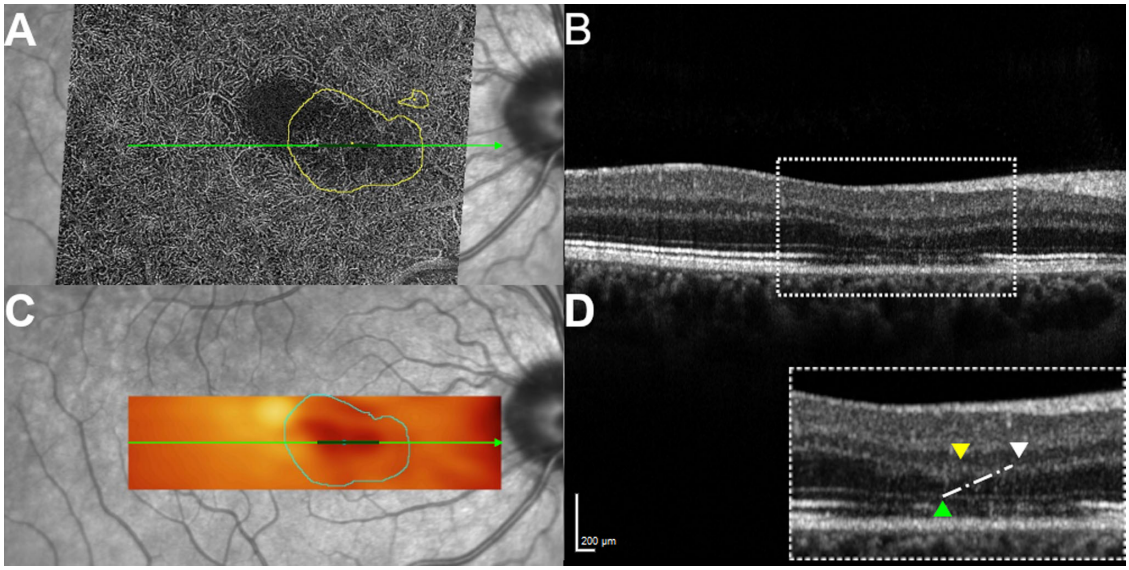

Figure 5. Outer nuclear layer (ONL) thickness in acute macular neuroretinopathy (AMN) lesions featuring persistent flow defects in optical coherence tomography angiography (OCTA) analysis. (**A**) Near infrared reflectance image of the fundus superposed with en face OCTA image of the DCP and AMN lesions corrected for Henle's fiber layer anatomy (*yellow*). (**B**) The B-scans corresponding to the *green line* in panel **A** shows a U-shaped pattern of ONL atrophy (*inset*). (**C**) Color thickness map superposition with uncorrected AMN lesion shows that ONL thickness is lower in the centroid of AMN lesion (*dark green line* indicates the area corresponding to the inset in *mosaic* **B**). (**D**) Magnified view of the inset shows a non-vertical correspondence (*dashed line*) between the point where ONL is lower (*green arrowhead*, centroid of uncorrected AMN lesion) and the capillary bare area in structural OCT (*white arrowhead*, centroid of corrected AMN lesion). DCP capillaries are pointed using *yellow arrowheads* and enable a direct comparison between normal capillaries and capillary bare areas (*white arrowheads*).

Discussion

In our analysis of 39 outer retinal lesions from 16 eyes with AMN, we identified 2 distinctive patterns of DCP alterations on OCTA and structural OCT B-scans co-localizing with individual AMN lesions. In nearly two thirds of AMN lesions, a central DCP draining venule was present (pattern 1), whereas in the remaining lesions there were central DCP flow defects within the lesion (pattern 2). Importantly, the detection of these patterns was significantly enhanced when correcting for physiological HFL radial orientation when correlating the outer retinal lesions of AMN with DCP anatomy. These findings support a role in the impairment of the capillary vortices and draining venules in the pathophysiology of AMN and demonstrate the importance of accounting for HFL anatomy (namely, the obliqueness of the photoreceptor axons and Müller cell fibers outside the foveola) when studying this entity.

Our findings are consistent with those of prior investigators who suggested that vascular events involving the DCP are involved in AMN.[13,18–24] Various studies have shown an association between absent or low-intensity flow within the DCP and photoreceptor disruption in other entities, including diabetic retinopathy, Purtscher's retinopathy, retinal venulitis, and retinal venous occlusive disease.[25–27] These observations appear to support that, although photoreceptors receive most of their nutritional support from the choroidal circulation, impairment of the DCP can cause photoreceptor inner segment loss, likely through axonal degeneration or Müller cell disruption.[5,22] The microcirculation within the human DCP has recently been evaluated using novel high-resolution imaging, showing inflow from intermediate capillary plexus (ICP) small arterioles and outflow through draining venules.[17,28] This in series connection hypothesis is supported by animal studies that demonstrated a watershed zone between the retinal and choroidal circulations at the OPL level,[29] and has been used to advocate for a vascular etiology in AMN.[30,31]

Our findings suggest that AMN lesions of less than one disk diameter co-localized with a capillary vortex in approximately 60% of the cases (pattern 1). This observation may have implications regarding mechanisms in diseases involving the DCP. The anatomic features of the DCP have been addressed recently using confocal microscopy.[28] The authors showed that DCP capillaries had a mean diameter of 6.9 µm and a laminar arrangement with numerous loops converging and forming a central draining venule, giving a vortex-like appearance.[28] Blood rheology in capillary plexuses is complex and determined by the interactions among plasma, geometry of the network, dynamics of blood cells, and the vessel wall.[32] Experimental studies have shown that flow velocity, hematocrit, and oxygen extraction are all reduced when plasma viscosity increases.[32] Others have shown that flow speed in the murine retina is affected by vascular branching morphology.[33] Whether the geometrical arrangement observed in capillary vortices and changes in blood viscosity secondary to oral contraceptives or viral infections impact oxygen delivery in the DCP has not yet been addressed.[34,35] We believe that this topic should be further studied, as it is likely to expand our understanding of the mechanisms involved in some AMN cases.

Another important finding in this study was the identification of DCP flow defects in approximately 30% of the cases (pattern 2). The detection of flow defects using OCTA has been used to support the hypothesis that capillary injury at the level of the DCP may be the primary etiology in AMN.[13,19,20,24] Using projection-resolved OCTA in a series of 5 eyes, Chu et al.[13] found reduced DCP flow signal over

Investigative Ophthalmology & Visual Science

5 AMN lesions and partial flow restoration within up to 6 weeks in the cases with follow-up. This finding coincided with the transition from OPL/ONL hyper-reflectivity to thinning of the ONL seen with structural OCT. The authors suggested that this could be explained by a transient vaso-occlusive event followed by reperfusion.[8] For this reason, our OCTA analysis was based on images acquired at the last follow-up available for each patient (median of 8 weeks). Our observations of flow defects that did not resolve within the follow-up period and the absence of structures resembling capillaries with structural OCT B-scans suggest a lasting vascular injury in the centroid of some AMN lesions. Our inability to detect draining venules over areas of flow defects may suggest that whatever is causing capillary damage may also be affecting the corresponding draining venules. However, interestingly, we detected capillary vortices and corresponding draining venules around the perimeter of the areas of flow defects. This seems to suggest that the DCP patterns herein described reflect different degrees of insult to capillary vortices, with pattern 2 being the more severe. The findings in pattern 2 might be interpreted as a decreasing gradient of flow changes expanding centrifugally from the location of the primary event (the centroid) toward the nearby draining vortices (see Fig. 4). If this hypothesis is correct, one would expect photoreceptor loss to be higher in the centroid of AMN lesions. Although limited to 10 lesions from 6 eyes, our analysis of ONL thickness maps supports this assumption and showed a strong inverse correlation ($r = 0.78$, $P < 0.001$) between areas with flow defect and ONL thickness, with the lowest ONL thickness noted at the centroid of these AMN lesions.

Strengths of this study included the correction for HFL Z-shape and high-quality images, including the use of High-Res OCT technology in four patients (36%). The High-Res OCT device allows the acquisition of OCT images with 3 µm axial resolution, which is double that of standard commercial SD-OCT devices and enables precise identification of retinal capillaries and venules.[17]

Limitations addressable in future studies include the small sample size and the lack of uniform follow-up durations. Imaging studies have demonstrated lateral extension of outer retinal changes in the first weeks after symptom onset in patients with AMN, likely representing the fusion of small adjacent lesions into larger ones.[5] Earlier imaging in some of the cases in our series might have impacted the lesion number and size. Additionally, the current study excluded seven AMN lesions that were larger than one disk diameter, so the generalizability of our findings to larger AMN lesions is unclear. However, given that larger AMN lesions may represent the gradual confluence of multiple smaller ones, analyzing the centroid of such larger lesions would pose methodological challenges and concerns. Draining venules are small structures with a median vascular diameter of 20 µm with OCT B-scans.[17] Thus, using structural OCT raster scans with an interscan distance greater than 20 µm might have impacted their detection. We also recognize the possibility of incorrect retinal layer segmentation. Although the segmentation of the retinal layers relevant for the study purpose was verified manually, we cannot exclude inaccuracies. ONL thickness was defined as the distance between the lower limit of the OPL and the ELM. As HFL exhibits directional reflectance, non-uniform OCT pupil light entry or HFL changes secondary to the AMN disease process may increase the reflectivity of this layer, making it more difficult to distinguish from the OPL.[7] For this reason, we excluded 4 out of the 39 AMN lesions from ONL thickness analysis.

Overall, this study supports the idea that adjusting for the displacement of bipolar and ganglion cells from the position of the cones in the perifovea may be relevant for a better understanding of AMN pathophysiology. Although there is already literature debating whether applying Drasdo displacement is necessary for structure-function relationships in glaucoma, to the best of our knowledge, this is the first application of this concept for better understanding AMN.[10,36,37] It should also be noted that the correction used to analyze the outer retinal lesions was based on the histologic measurements of HFL available in the literature, which are limited to the horizontal meridian.[10] We also acknowledge that differences in retinal magnification were not included in this process, nor were the characteristics of the foveal cones (foveal pit size and peak foveal cone density) taken into account in our analyses. Thereby, our approach did not consider inter-person and inter-meridian variability, which would be necessary for a more precise transformation of the data and thus impact the accuracy of our results.[12] However, to the best of our knowledge, an algorithm able to perform a personalized correction for HFL anatomy using noninvasive imaging has not been yet been developed.[7,11,12] Whereas corrected AMN lesions showed good correspondence to areas of DCP nonperfusion, suggesting that the calculi were adequate (see Fig. 4), this does not exclude the possibility of confirmation bias. Finally, our study did not aim to determine the specific mechanisms contributing to the development of AMN. Although our findings support the involvement of the DCP in AMN pathophysiology, they do not shed any light on whether DCP involvement is the primary event (i.e. vaso-occlusive) or secondary to OPL damage (i.e. an inflammatory event).

In conclusion, we observed a high prevalence of either a capillary vortex or flow defects within the centroid of AMN lesions. AMN lesions associated with flow defects were associated with lower ONL thickness values during the follow-up period. These associations could not be detected without correcting the projection of outer retinal changes in the DCP for HFL anatomy. Our analysis supports a distal insult at the level of the capillary vortices in AMN.

Acknowledgments

Supported by The Macula Foundation Inc., New York, New York, USA. D.C. was supported in part by a studentship from Fundação Luso-Americana para o Desenvolvimento (FLAD, USA R&D@PhD – Proj 2020/0140). P.R. was supported by The Philippe Foundation.

Disclosure: **D. Cabral**, None; **P. Ramtohul**, None; **L. Zatreanu**, None; **D. Galhoz**, None; **M. Leitao**, None; **V. Noguerira**, None; **D. Sarraf**, Amgen (California, USA) (C, F), Boehringer (F), Genentech (San Francisco, California) (C, 400F), Heidelberg (Heidelberg, Germany); (F), Iveric Bio (C), Novartis (Basel, Switzerland) (C, F), Optovue (California, USA) (C, F), Regeneron (NY, USA) (F), Bayer (Berlin, Germany) (C, F), Topcon (Tokyo, Japan) (F); **K.B. Freund**, Genentech (San Francisco, California) (C), Optovue (California, USA) (C), Zeiss (Dublin, USA) (C), Heidelberg Engineering (Heidelberg, Germany) (C), Allergan Inc. (Irvine, California, USA) (C), Bayer (Berlin, Germany) (C), Novartis (Basel, Switzerland) (C), Genentech (San Francisco, California) (F), Roche (Basel, Switzerland) (F)

References

1. Bos PJM, Deutman AF. Acute macular neuroretinopathy. *Am J Ophthalmol*. 1975;80(4):573–584.
2. Corver HD, Ruys J, Kestelyn-Stevens AM, de Laey JJ, Leroy BP. Two cases of acute macular neuroretinopathy. *Eye*. 2007;21(9):1226–1229.
3. Feigl B, Haas A. Optical coherence tomography (OCT) in acute macular neuroretinopathy. *Acta Ophthalmol Scand*. 2000;78(6):714–716.
4. Monson BK, Greenberg PB, Greenberg E, Fujimoto JG, Srinivasan VJ, Duker JS. High-speed, ultra-high-resolution optical coherence tomography of acute macular neuroretinopathy. *Br J Ophthalmol*. 2007;91(1):119–120.
5. Fawzi AA, Pappuru RR, Sarraf D, et al. Acute macular neuroretinopathy: long-term insights revealed by multimodal imaging. *Retina*. 2012;32(8):1500–1513.
6. Hansen SO, Cooper RF, Dubra A, Carroll J, Weinberg DV. Selective cone photoreceptor injury in acute macular neuroretinopathy. *Retina*. 2013;33(8):1650–1658.
7. Lujan BJ, Roorda A, Knighton RW, Carroll J. Revealing Henle's fiber layer using spectral domain optical coherence tomography. *Invest Ophthalmol Vis Sci*. 2011;52(3):1486–1492.
8. Stone J, van Driel D, Valter K, Rees S, Provis J. The locations of mitochondria in mammalian photoreceptors: Relation to retinal vasculature. *Brain Res*. 2008;1189(1):58–69.
9. Kar D, Kim YJ, Packer O, Dacey DM, Curcio CA. Morphological variants of mitochondria in neurons surrounding the deep capillary plexus in human retina. *Invest Ophthalmol Vis Sci*. 2021;62(8):2220.
10. Drasdo N, Millican CL, Katholi CR, Curcio CA. The length of Henle fibers in the human retina and a model of ganglion receptive field density in the visual field. *Vision Res*. 2007;47(22):2901–2911.
11. Ramtohul P, Cabral D, Sadda S, Freund KB, Sarraf D. The OCT angular sign of Henle fiber layer (HFL) hyperreflectivity (ASHH) and the pathoanatomy of the HFL in macular disease. *Prog Retin Eye Res*. 2022;101135.
12. Masri RA, Grünert U, Martin PR. Analysis of parvocellular and magnocellular visual pathways in human retina. *J Neurosci*. 2020;40(42):8132–8148.
13. Chu S, Nesper PL, Soetikno BT, Bakri SJ, Fawzi AA. Projection-resolved OCT angiography of microvascular changes in paracentral acute middle maculopathy and acute macular neuroretinopathy. *Invest Ophthalmol Vis Sci*. 2018;59(7):2913–2922.
14. Crowston JG, Hopley CR, Healey PR, Lee A, Mitchell P. The effect of optic disc diameter on vertical cup to disc ratio percentiles in a population based cohort: The Blue Mountains Eye Study. *Br J Ophthalmol*. 2004;88(6):766–770.
15. Schindelin J, Arganda-Carreras I, Frise E, et al. Fiji: an open-source platform for biological-image analysis. *Nat Methods*. 2012;9(7):676–682.
16. Galhoz D. AMN Lesion Masks Distortion. Published September 2022. Accessed October 9, 2022. Available at: https://github.com/DanielGalhoz/AMN-Lesion-Masks-Distortion.
17. Cabral D, Fradinho AC, Pereira T, et al. Macular Vascular Imaging and Connectivity Analysis Using High-Resolution Optical Coherence Tomography. *Transl Vis Sci Technol*. 2022;11(6):2.
18. Azar G, Wolff B, Cornut PL, Sahel JA, Mauget-Faÿsse M. Spectral domain optical coherence tomography evolutive features in acute macular neuroretinopathy. *Eur J Ophthalmol*. 2012;22(5):850–852.
19. Liu JC, Nesper PL, Fawzi AA, Gill MK. Acute macular neuroretinopathy associated with influenza vaccination with decreased flow at the deep capillary plexus on OCT angiography. *Am J Ophthalmol Case Rep*. 2018;10:96–100.
20. Hwang CK, Sen HN. Concurrent vascular flow defects at the deep capillary plexus and choriocapillaris layers in acute macular neuroretinopathy on multimodal imaging: A case series. *Am J Ophthalmol Case Rep*. 2020;20:100866.
21. Nemiroff J, Sarraf D, Davila JP, Rodger D. Optical coherence tomography angiography of acute macular neuroretinopathy reveals deep capillary ischemia. *Retin Cases Brief Rep*. 2018;12(1):S12–S15.
22. Pecen PE, Smith AG, Ehlers JP. Optical coherence tomography angiography of acute macular neuroretinopathy and paracentral acute middle maculopathy. *JAMA Ophthalmol*. 2015;133(12):1478–1480.
23. Casalino G, Arrigo A, Romano F, Munk MR, Bandello F, Parodi MB. Acute macular neuroretinopathy: Pathogenetic insights from optical coherence tomography angiography. *Br J Ophthalmol*. 2019;103(3):410–414.
24. Ramtohul P, Comet A, Denis D. Optical Coherence Tomography Angiography Recovery Pattern of Acute Macular Neuroretinopathy. *JAMA Ophthalmol*. 2020;138(2):221.
25. Scarinci F, Nesper PL, Fawzi AA. Deep Retinal Capillary Nonperfusion Is Associated with Photoreceptor Disruption in Diabetic Macular Ischemia. *Am J Ophthalmol*. 2016;168:129–138.
26. Iovino C, Au A, Ramtohul P, et al. Coincident PAMM and AMN and Insights into a Common Pathophysiology. *Am J Ophthalmol*. 2022;236:136–146.
27. Ramtohul P, Freund KB. Clinical and Morphological Characteristics of Anti–Programmed Death Ligand 1–Associated Retinopathy. *Ophthalmol Retina*. 2020;4(4):446–450.
28. An D,, Yu P,, Freund KB,, et al . Three-Dimensional characterization of the normal human parafoveal microvasculature using structural criteria and high-resolution confocal microscopy. *Invest Ophthalmol Vis Sci*. 2020;61(10):3.
29. Ahmed J, Braun RD, Dunn R, Linsenmeier RA. Oxygen Distribution in the Macaque Retina. *Invest Ophthalmol Vis Sci*. 1993;34(3):516–521.
30. Turbeville SD, Cowan LD, Gass JDM. Acute Macular Neuroretinopathy. *Surv Ophthalmol*. 2003;48(1):1–11.
31. Bhavsar KV, Lin S, Rahimy E, et al. Acute macular neuroretinopathy: A comprehensive review of the literature. *Surv Ophthalmol*. 2016;61(5):538–565.
32. Pries AR, Secomb TW, Gaehtgens P. Biophysical aspects of blood flow in the microvasculature. *Cardiovasc Res*. 1996;32(4):654–667.
33. Mirzapour-Shafiyi F, Kametani Y, Hikita T, Hasegawa Y, Nakayama M. Numerical evaluation reveals the effect of branching morphology on vessel transport properties during angiogenesis. Beard DA, ed. *PLoS Comput Biol*. 2021;17(6):e1008398.
34. Nader E, Nougier C, Boisson C, et al. Increased blood viscosity and red blood cell aggregation in patients with COVID-19. *Am J Hematol*. 2022;97(3):283–292.
35. Lowe GDO, Drummond MM, Forbes CD, Barbenel JC. Increased blood viscosity in young women using oral contraceptives. *Am J Obstet Gynecol*. 1980;137(7):840–842.
36. Tong J, Phu J, Alonso-Caneiro D, Khuu SK, Kalloniatis M. Clinical Evaluations of Macular Structure-Function Concordance With and Without Drasdo Displacement. *Transl Vis Sci Technol*. 2022;11(4):18.
37. Giammaria S, Sharpe GP, Dyachok O, et al. Elucidating macular structure–function correlations in glaucoma. *Sci Rep*. 2022;12(1):10621.

Investigative Ophthalmology & Visual Science